ELSEVIER

Physica C 265 (1996) 126–134

PHYSICA C

Flat $YBa_2Cu_3O_{7-x}$ layers for planar tunnel-device technology

C. Klemenz, H.J. Scheel *

Cristallogenèse, Institute of Micro- and Optoelectronics, Swiss Federal Institute of Technology, Ch. de Bellerive 34, CH-1007 Lausanne, Switzerland

Received 31 October 1995; revised manuscript received 13 March 1996

Abstract

The conditions for achieving extremely flat $YBa_2Cu_3O_{7-x}$ (YBCO) surfaces with large interstep distances as required for a reliable planar HTSC tunnel-device technology are analyzed. Considerations of thermodynamics, kinetics and transport of the growth species show that by liquid phase epitaxy (LPE) it is possible to achieve such flat YBCO surfaces, which is experimentally proven. Specifically, in LPE the growth from relatively concentrated solutions occurs at high temperatures near thermodynamic equilibrium. The small supersaturation (of < 0.17°C) required for obtaining step distances of more than 10 μm has been calculated by using the heat of solution from the measured solubility curve and the theoretical treatment of the experimental surface features. Jackson's α factors (roughness parameter) are derived for *a*- and *c*-oriented YBCO films and explain the different degree of polygonization of the observed growth spirals. The concentrations of YBCO in physical vapour deposition (PVD) and in metal-organic chemical vapour deposition (MOCVD) are very small and the supersaturations at least 10^2 times higher than in LPE. This, together with the thermodynamic stability limit (temperature, oxygen partial pressure), sets an inherent limit to the interstep distance in PVD and MOCVD, thus limiting the achievable flatness of vapour-grown YBCO layers.

1. Introduction

For tunnel-device applications of high-T_c superconductivity (HTSC), extremely flat surfaces are required because of the very short coherence lengths of HTSC compounds. The majority of HTSC layers have been grown so far from the vapour phase, either by physical vapour deposition (PVD) like sputtering or laser ablation, or by metal-organic chemical vapour deposition (MOCVD). Thereby high critical temperatures T_c and high critical current densities J_c could be achieved, but not the surface flatness required for a reliable planar technology for SQUIDs and digital applications.

The potential to achieve quasi atomically flat surfaces by liquid-phase epitaxy (LPE) is well-known for GaAs [1–3]. In LPE, growth occurs near to equilibrium, i.e. at low supersaturation, which allowed the growth of NdBCO and YBCO layers with layer propagation over macroscopic dimensions for the first time [4]. In that reference also the earlier attempts to apply LPE for high-T_c superconductors are reviewed. Whereas vapour-deposited YBCO layers show a high screw dislocation density of the order of $10^9/cm^2$ with interstep distances of typically 30 nm [5–7], layers grown by liquid phase epitaxy have a macrospiral density of 5×10^2 to $10^4/cm^2$ and interstep distances up to 3 μm [8].

* Corresponding author. Fax: +41 21 693 4750.

PII S0921-4534(96)00214-6

However, this requires a precise control of the growth parameters which is very delicate. Especially the supersaturation adjustment is one of the most important factors for achieving high-quality layers with large interstep distances. Since it is very difficult to know the supersaturation during the growth procedure (variation of the liquidus/compositional changes of the melt due to crucible corrosion), an attempt was made in the present work to calculate the supersaturation from growth features (growth spirals) on LPE layers, in order to estimate the supersaturation necessary to achieve more than 10 μm distance between monosteps as required for a planar HTSC tunnel-device technology. For this estimation first the heat of solution was derived, and compared with known values of the heat of melting. The supersaturation could then be estimated for a 4-fold spiral grown by LPE [8], and calculated for single spirals in function of interstep distances. The size of the critical nucleus was roughly estimated from the shape of the spiral, and compared with the theory.

In the second part the surface morphologies of PVD-, MOCVD- and LPE-grown layers are compared and the strengths and limitations of the epitaxial growth techniques discussed. Finally, a combined LPE and PVD/CVD technology is suggested for development of planar tunnel-device structures.

2. Derivation of the heat of solution

The driving force for growth from solution is related to the undercooling $\Delta T = T_e - T$, with T the actual and T_e the equilibrium temperature. The supersaturation can also be expressed by the change in Gibbs free energy of the system $\Delta\mu = \Delta H - T\Delta S$, where ΔH and ΔS are the differences in the enthalpy and entropy of the crystalline and fluid phases. Near equilibrium, $\Delta\mu \approx 0$, so that ΔS can be eliminated:

$$\Delta\mu = \Delta H\left(1 - \frac{T}{T_e}\right) \approx \Delta H\left(\frac{\Delta T}{T_e}\right).$$

Since the volume change on melting is small, ΔH may be approximated by the heat of solution L_{sol} [9,10].

The heat of solution can be calculated from equilibrium data obtained at varying concentrations of the solute (YBCO) in the solvent ($BaCuO_2$/CuO flux), according to

$$L_{sol} = RT^2 \frac{d\ln(c_{sat})}{dT}$$

or

$$L_{sol} = 4.574 T_1 T_2 \frac{\log c_{sat(1)} - \log c_{sat(2)}}{T_1 - T_2}, \qquad (1)$$

where L_{sol} is the constant partial heat of saturated solution over the temperature range T_1 to T_2 and the concentration range $c_{sat(1)}$ to $c_{sat(2)}$. Eq. (1) is restricted to regular solutions, which implies that it may be used for rather dilute solutions with no significant interactions between solute and solvent.

According to our refined (from Ref. [4]) experimental solubility curve, for $YBa_2Cu_3O_{7-x}$ crystals with $x \approx 0.8$, grown in air ($P_{O_2} = 0.2$ atm) in a $BaCuO_2$/CuO flux containing 31 mol.% BaO, we obtain $L_{sol} = 34.7$ kcal/mol at 1273 K. This value is in good agreement with the data of Tsagareisvili et al. [11,12] who give for the enthalpy of melting ΔH_{melt} of $YBa_2Cu_3O_6$ at 1446 K a value of 36.44 kcal/mol and for $YBa_2Cu_3O_7$ at 1503 K a value of 41.03 kcal/mol. For an undercooling ΔT of 0.5°C, the Gibbs free energy difference ΔG would then be $\Delta G_{(\Delta T = 0.5)} = 13.6$ cal/mol, and for $\Delta T = 2.5$°C (typical value, see below) $\Delta G_{(\Delta T = 2.5)} = 68.1$ cal/mol, which is in good agreement with a previous estimation [13].

3. Spiral growth

Fig. 1 shows a 4-fold spiral on a YBCO (001) surface grown by LPE [8]. On this surface, the density of growth hillocks is about $5 \times 10^2/cm^2$ to $10^4/cm^2$. The macrospirals show a hollow core in the centre, and a clear dependence of interstep distances to step heights. Such hollow dislocations have large Burgers vectors and were predicted by Frank [14], and a model was proposed for their formation, based on a combination of block crystals [15].

In order to calculate the size of the radius of the critical nucleus on this surface, the lengths of the

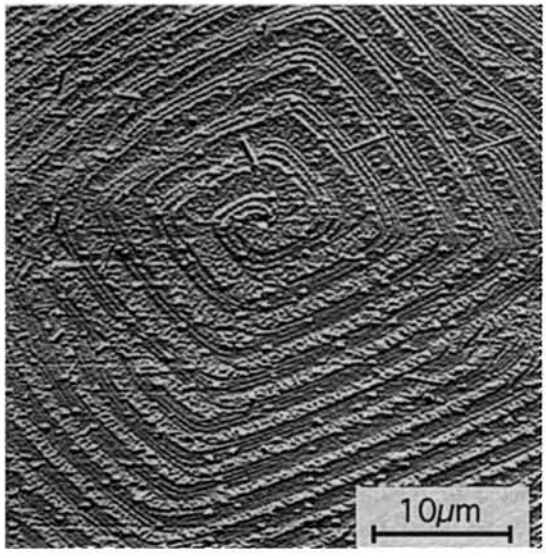

Fig. 1. Polygonized spiral with a hollow core seen by atomic force microscopy [8]. The interstep distance is about 1.95 μm and the steps are composed of 4 to 5 monosteps of about 12 Å height.

successive arms of this 4-fold spiral were measured and compared, since this distance is an integer of the radius ρ_c of the critical 2D nucleus, as shown in Fig. 2. A rough estimation gives $\rho_c \approx 450$ nm. Recent measurements of pulsed laser deposited films [7] gave a value of a critical nucleus $\rho_c = 2.4$ nm, which is nearly 200 times smaller than on LPE films.

Burton, Cabrera and Frank (BCF) [16] showed that a screw dislocation induces a spiral with an interstep distance $y_0 = 4\pi\rho_c/\epsilon$, where in the case of a group of dislocations of the same sign, ϵ can be as great as the number of dislocations contained in it.

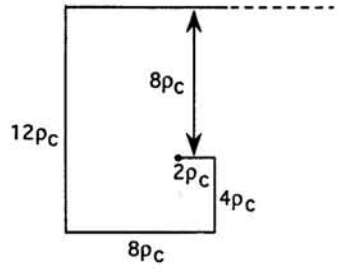

Fig. 2. Schematic view of a fully polygonized spiral. The successive arms of the spiral and the interstep distance are an integer of the radius ρ_c of the critical 2D nucleus.

Cabrera and Levine [17] gave an improved approximation of the interstep distance $y_0 = 19\rho_c$ for a single spiral, thus $y_0 = 19\rho_c/\epsilon$ for a bundle of dislocations. Mutaftschiev [18] suggested an interstep distance of a fully polygonized spiral $y_0 = 8\rho_c$. It should also be mentioned that polygonized spirals may grow by a different mechanism than round ones, since a smooth edge has less kink sites for attachment of growth units. In the spiral of Fig. 1, the radius of the hollow core is $r_{hc} \approx 230$ nm. It should be noted that the radius of the hollow core does not depend on volume or surface diffusion of growth units. It depends only on the supersaturation at the solid–liquid interface and on the stress field [19]. On the other hand, the depth of the hollow core will be limited by volume diffusion.

4. Supersaturation

The interstep distance for an Archimedean spiral may be related to the supersaturation by [17]

$$y_0 = \frac{19\gamma_m a}{kT\sigma}. \tag{2}$$

In case of solution growth, the energy per growth unit (or molecule) γ_m on the edge of the critical nucleus is of the order of 1/6 of the heat of solution per molecule [20]. $\sigma = \Delta n/n_e = (n - n_e)/n_e$ is the relative supersaturation, with n and n_e the actual and the equilibrium concentrations of the solute, and a the length of the growth unit.

We have measured the interstep distance and the step height for 9 (not fully) polygonized spirals with bunched steps grown on the same surface ($NdGaO_3$ (110) substrate) [8]. If we assume that the supersaturation over this small area of about 1 mm^2 is nearly equal, our experimental results show that the multiplicity m of the spirals, inducing the corresponding m-fold activity of the stepped edges, must be taken in account as following:

$$y_0 = \frac{19\gamma_m am}{kT\sigma} \tag{3}$$

and the mean undercooling over this surface is then about 3 ± 0.5°C (a typical example is given below). We do not consider here the anisotropy of γ_m, which will be higher on low energy planes.

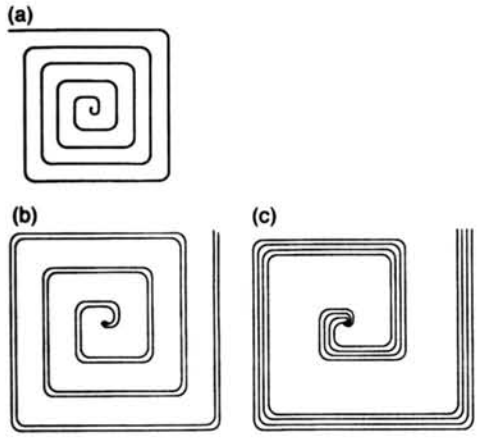

Fig. 3. (a) Single spiral with monosteps. (b) Spiral with double bunched steps. (c) Spiral with 4-fold bunched steps.

In Fig. 3 the difference of interstep distances between the single spiral (a) with monosteps and with spirals (b) (double bunched steps) and (c) (4-fold bunched steps) is shown for the same supersaturation. Fig. 3 based on experimental results indicates that the integral step density, i.e. step length per unit area, is the same for a given (high) supersaturation in the diffusion-limited growth regime.

For example, for spiral No. 034 [8], for $\gamma_m = 4.01 \times 10^{-20}$ J, $a = 3.9$ Å ($a = b$ for tetragonal YBCO at 996°C), $m = 5$, $y_0 = 3.1$ μm, the supersaturation is $\sigma = 0.027$. With $\sigma = \Delta n/n_e$, according to the solubility of YBCO in the $BaCuO_2/CuO$ flux, this corresponds to an undercooling $\Delta T \approx 2.7$°C.

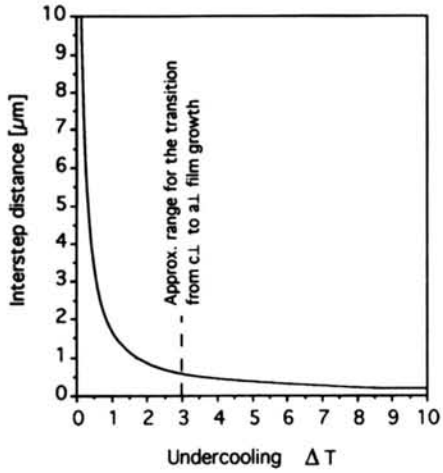

Fig. 4. Interstep distances y_0 versus undercooling ΔT according to the BCF theory with data from the solubility curve of YBCO in the $BaCuO_2/CuO$ flux at 31 mol.% BaO.

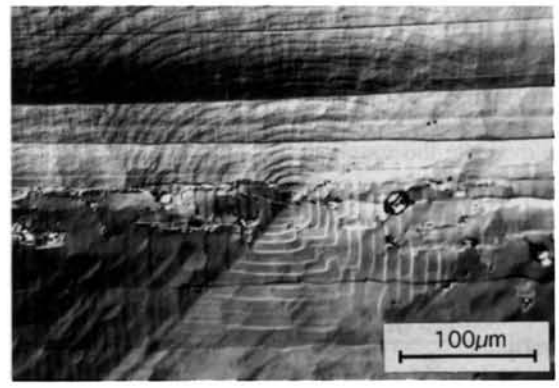

Fig. 5. Macrospiral at the boundary of a- and c-oriented YBCO layer seen by differential interference contrast (Nomarski) microscope. The polygonization occurred on the c region, whereas rounded macrosteps continues on the a region, showing that $\alpha_{(001)} > \alpha_{(100)}$.

This relation is shown in Fig. 4: the supersaturation $\sigma = \Delta n/n_e$ is calculated for different interstep distances, assuming a single spiral. The corresponding undercooling is calculated with the solubility curve. One can see from Fig. 4 that a supersaturation (and a precise supersaturation control) $\Delta T < 0.17$°C is needed in order to achieve a single spiral with interstep distances > 10 μm as required for planar HTSC technology.

On (110) $NdGaO_3$ substrates, depending on the supersaturation and other parameters, either c, a or mixed YBCO layers can be grown by LPE [8,21]. Fig. 5 is a Nomarski differential interference contrast microphotography of a macrospiral which could develop at a boundary region between c- and a-orientation. Polygonization occurred on the c-oriented region ($[001]_{YBCO}$ ⊥ to $(110)_{substrate}$), whereas rounded macrosteps continued on the a/b-oriented ($[100]/[010]_{YBCO}$ ⊥ to $(110)_{substrate}$) side. It should be noted that the degree of polygonization of a spiral does not only depend on the supersaturation, but impurities as well as the substrate (stress field) may have a significant effect.

5. Surface roughness

When a spiral step is smooth, with a low kink density, the advancing rate is controlled by the

stronger bonds within the face, according to the PBC theory [22]. The spiral tends then to take a polygonal morphology, whose symmetry corresponds to the symmetry of the face. Jackson's α factor [23] allows to evaluate the roughness of an interface as follows:

$$\alpha_{(hkl)} = \xi_{(hkl)} \frac{L}{kT},$$

where

$$\xi_{(hkl)} = \frac{E_{\mathrm{slice}(hkl)}}{E_{\mathrm{cr}}},$$

with $E_{\mathrm{cr}} = E_{\mathrm{slice}} + E_{\mathrm{att}}$. E_{slice} is the energy of a growth unit within a slice, as defined in the Hartman–Perdok theory [22], E_{cr} the crystallization energy and E_{att} the attachment energy. These energies depend on the surface (hkl) considered. L is the heat of the transformation. In case of solution growth, L represents the heat of solution per molecule. Sun et al. [24] have calculated E_{att} and E_{cr} of YBCO by using the point charge model, and Van de Leemput et al. [25] by using the PBC theory. The geometrical factor was then calculated by Yamada et al. [26] using their data. It was found that $\alpha_{(100)}/\alpha_{(001)}$ is about 0.9 with data from Ref. [24] and 0.75 with Ref. [25]. For $YBa_2Cu_3O_{7-x}$ with $x \approx 0.9$, the geometrical factors are $\xi_{(001)} \approx 0.966$ and $\xi_{(100)} \approx 0.726$ [25]. By using $L_{\mathrm{sol}} = 2.41\mathrm{x}10^{-19}$ J/molecule at 1000°C and the values of Ref. [25], we obtain

$$\alpha_{(001)} \approx 13.25 \text{ and } \alpha_{(100)} \approx 9.96.$$

Thus, the (001) face is smoother than the (100) face, as it is confirmed by the degree of polygonization of the spiral of Fig. 5.

6. Comparison of PVD- and LPE-grown surfaces

Both *a*- and *c*-oriented YBCO layers were obtained by LPE as well as by PVD. In the latter case a temperature dependence was established: *a* layers at low growth temperatures, mixed *a*/*c* layers at 750–800°C, and pure *c* layers above a transition range at around 825°C (Mukaida and Miyazawa [27]). These results are in agreement with the model of Pennycook et al. [28] that YBCO *a* layers are kinetically favoured, whereas the thermodynamically preferred *c* layers grow at higher temperatures. STM measurements [29] revealed step heights between 0.2 and over 20 nm. In PVD and CVD there seems to be a coincidence of the density of 2-dimensional islands (nuclei), expected from the measured interstep distances, and the density of spiral islands observed by STM [5–7], thereby suggesting the formation of spiral islands by coalescence of misaligned first-nucleated 2D islands [30].

Interstep distances are typically 20 nm and rarely exceed 50 nm when high growth temperatures are applied. It was suggested [13] that in these cases near the thermodynamic stability limit (temperature, P_{O_2}), liquid-assisted growth, quasi by a vapour–liquid–solid VLS mechanism, would allow large interstep distances in PVD or CVD. Here it should be mentioned that island formation and thus spiral island formation can be suppressed by substrate misorientation. When the interstep distance of the misorientation steps is smaller than $19\rho_c$ for the specific supersaturation conditions, which corresponds in PVD and CVD to misorientation angles between 3° and 5° [30–32], the island formation can be prevented and a pure step-flow mode achieved.

The quasi inherent limits of interstep distances below 100 nm in vapour epitaxy of YBCO could be explained by the incongruent evaporation [1] of the compound. This composition is thermodynamically not stable and therefore, in analogy with incongruent melting, it decomposes before or upon evaporation. The advantage of the growth of incongruent melting compounds from high-temperature solutions [20] is that large perfect crystals and epitaxial layers can be grown below the decomposition temperature because of relatively high concentration and the adjustable very low supersaturation. In the case of vapour deposition the supersaturation cannot be expressed in terms of the partial pressure of YBCO(g), because the gas phase will contain other species depending on thermodynamics. The chemical potential can be expressed by the rate-limiting component of the gas phase which in general will be the species with the

[1] There is an analogy with GaAs (also shows incongruent evaporation) and its quasi inherent limit of interstep distances around 200 nm in MBE growth, whereas in vapour growth of silicon, step distances above 1 μm were observed at high growth temperatures.

lowest vapour pressure (unless the process is controlled by the ratio of the flux of the different species).

The small interstep distances in PVD and CVD demonstrate the very high supersaturation (whatever its definition in this case), whereas the concentration of YBCO-derived species is very low (many orders of magnitude lower than in LPE) so that the deposition rate for epitaxial films is low, typically 0.1 nm/s.

The relatively low growth temperatures in PVD and CVD of YBCO (which are limited by its thermodynamic stability) also limit surface diffusion as factor to enhance interstep distance. The incongruent evaporation of YBCO also explains the difficulty to achieve precise control of the cation stoichiometry, and the formation of high defect densities in vapour-grown YBCO layers.

In liquid phase epitaxy the situation is quite different: the concentration of solute is high ($\sim 5 \times 10^{-2}$ compared to $< 10^{-8}$ in PVD), the temperature is high ($\sim$ 1000°C), and the supersaturation can be adjusted to be very low (see above). Therefore a high growth rate (1–50 nm/s) can be applied depending on the hydrodynamically controlled thickness of the diffusion boundary layer [20,33]. Y–Ba–Cu–O complexes diffuse to the steps at the surface, either directly or with participation of surface diffusion [34,35], react there to form the layer structure of YBCO, and the excess Ba–Cu–O (the solvent fraction) moves away from the growth interface. In this near-equilibrium growth the transition from the misoriented substrate to the facet, the equilibrium surface occurs [1,3] where steps propagate from step sources like screw dislocations or other defects.

The so far observed interstep distances in LPE of YBCO between 0.3 and 17 μm correspond to the low supersaturation as discussed above. Normally this supersaturation is made so small that island formation by 2D nucleation can be suppressed. There is no inherent limit for the interstep distance in LPE; it could be mm or even cm if the technological prerequisites are established.

7. Comparison of liquid and vapour phase epitaxy

In epitaxy from the liquid phase thermodynamics is the dominating factor. The driving force for growth is determined by the enthalpy of melting (which is nearly equal to the heat of solution) and can be adjusted by the undercooling ΔT of the solution. The solution consists of "solvated" complexes containing the constituents of the crystalline phase [20]. These complexes diffuse towards the steps of the growth interface where desolvation occurs, and solvent species diffuse away from the interface [20]. Kinetics, i.e. the growth rate, is normally limited by mass transport through the diffusion boundary layer. Thus, by substrate rotation, an increased maximum stable growth rate (> 10 nm/s) can be applied and simultaneously the solution homogenized.

In epitaxy of YBCO from the vapour phase, kinetics is the dominating factor since the concentration of YBCO species in vacuum or vapour is infinitesimal. Metal or metal–oxygen species arriving through the vapour successively react at the surface and at the step to form the YBCO layer structure. In the case of congruent evaporation the driving force for condensation would be given (besides the flux species) by the enthalpy of sublimation which for numerous compounds is about ten times higher than the enthalpy of melting, an important difference. Since in case of YBCO there are only constituent metal–oxygen species, the definition of supersaturation from equilibrium pressure of YBCO over the solid and actual pressure of YBCO is not possible [36].

The liquid-assisted growth from the vapour phase, near the thermodynamic stability limit of YBCO discussed before to explain the largest interstep distances in PVD and MOCVD, can be regarded as an intermediate case, where both the enthalpies of melting and of sublimation contribute as driving force for epitaxy.

In addition to these fundamental differences between epitaxy from liquid and vapour phases there are a number of other distinguishing factors.

An important difference are the substrate requirements. In PVD/MOCVD the misfit of substrates or of buffer layers plays a certain role for T_c and J_c [37], but epitaxial growth and relatively high critical current densities have been achieved even on substrates with more than 2% misfit. Anyhow, one cannot expect flat surfaces. When, however, extremely flat surfaces are to be achieved in LPE then the misfit should be extremely small, less than 0.1%

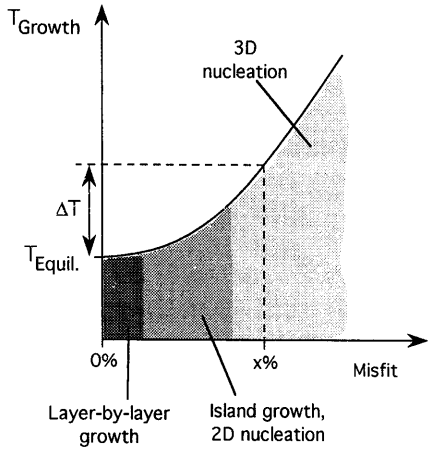

Fig. 6. Supersaturation versus misfit for the different growth modes. Only a small misfit with a small undercooling will allow layer-by-layer growth over large distances. A large misfit of $x\%$ requires a high supersaturation ΔT for growth.

[38]. Only at practically zero misfit the layer-by-layer (Frank–van der Merwe) growth mode can be expected as shown by molecular dynamics studies [39]. In addition is the supersaturation required to initiate heteroepitaxial growth increasing with misfit, thereby exceeding the low supersaturation necessary for the large interstep distances as discussed above. This relation supersaturation ($T_{\text{Growth}} - T_{\text{Equil.}}$) versus misfit is shown schematically in Fig. 6, along with the ranges of the different growth modes. This plot is in analogy with the diagram of Grabow and Gilmer [39] who showed the effect of adhesion energy and misfit on the growth modes.

Therefore, substrate–superconductor systems with extremely small misfit have to be found in order to achieve flat surfaces. But also the thermal expansion differences should be small, less than 10%, in order to prevent excessive strain and cracking upon cooling from epitaxial growth temperature [38]. There are still more requirements for substrates to be used in LPE: they should have a high chemical stability so that they are not corroded or dissolved in the quite aggressive high-temperature solutions of YBCO at around 1000°C. Furthermore should the substrates have a small misorientation with the ideal crystallographic plane, less than 0.1°, so that transition to faceting, to the equilibrium surfaces with large interstep distances, can be achieved [1,3].

The cation stoichiometry, the 1:2:3 ratio, is automatically adjusted in LPE by thermodynamics, whereas in PVD and CVD a reliable accurate stoichiometry control is quite demanding, even in sputtering at relatively high oxygen pressures using targets of defined cation ratio.

The oxidation behaviour is also different: PVD- and MOCVD-grown layers of *a*- or *c*-orientation are easily oxidized, mostly in situ during cooling to room temperature, due to the rough surfaces and the structural defects like grain boundaries, dislocations etc. The pronounced anisotropy of the oxygen diffusion coefficients ($D\|[010] \gg D\|[100] \gg D\|[001]$) facilitates oxidation of LPE-grown *a* layers, whereas the oxidation of the structurally quite perfect *c* layers is similarly difficult as that of high-quality bulk crystals [13]. Thereby show LPE-grown *a* layers characteristic features due to (110) twinning caused by the tetragonal–orthorhombic phase transformation [21], whereas LPE-grown *c* layers can be easily recognized by typical crossed (tweed-like) twin patterns [8].

Another significant difference between PVD/MOCVD and LPE is the critical current density J_c whereas T_c can be high (92 K for YBCO) in both cases. The structural defects of vapour-grown layers lead to generally high J_c values between 10^6 to about 5×10^7 A/cm^2 at 77 K [37] as long as the layers are compact and at least highly textured, with non-excessive secondary phases. The LPE-grown layers can be quite perfect so that due to weak pinning the J_c values are of the order of 5×10^2 to 10^4 A/cm^2 [21], corresponding to single crystals which are grown under similar conditions from high-temperature solutions. However, Yoshida et al. [40] have measured high J_c of 1.1×10^5 A/cm^2 which can be explained by the large misfit with the MgO substrates applied.Thus, LPE-grown layers are directly useful for low-J_c applications. Furthermore, by irradiation after growth artificial pinning defects can be introduced to enhance J_c.

There are also practical differences, for instance in LPE crucibles are required leading to contamination from crucible corrosion [41] which, however, could be resolved with the development of Y_2O_3 crucibles [42] now commercially available [13]. The LPE apparatus can be quite simple with a muffle or tube furnace with rotation and translation of sub-

strates; for adjustment of the small supersaturation a precise control of temperature and temperature gradients is required ($\pm < 0.1$°C, respectively $\pm \sim$ 1°C/cm) at around 1000°C growth temperature. In contrast to PVD (which has been achieved in numerous physics laboratories) is LPE quite a complex and sensitive process which requires great expertise in crystal growth science and technology.

8. Conclusions

The following summary has been made for YBCO. The situation may be somewhat different for Bi- and Tl-based superconductors of higher T_c with their mica-like layer structures and problems of chemical polytypism. For YBCO and other 123 compounds one could conclude from a crystal grower's standpoint, that PVD and MOCVD will in future be useful for numerous high-J_c applications where neither surface flatness nor layer homogeneity for patterning/device processing nor well-defined low surface resistance are needed, and where also yield and reliability of devices are not critical factors. The most promising approach to achieve relatively homogeneous and flat layers of YBCO on large diameter substrates is that of Kinder et al. [43].

The potential of LPE lies in the fabrication of base electrodes with quasi atomically flat surfaces and also for extremely thin pinhole-free barrier layers for tunnel devices. The (patterned) top electrode can be more conveniently deposited by PVD or MOCVD at lower growth temperatures. This combined technology is needed for a reliable planar technology in fabrication of SQUIDs and integrated tunnel devices at high yield with minimum scatter of device characteristics.

LPE has been the technology for achieving the first semiconductor lasers and for achieving now the highest performance optoelectronic devices. LPE has also been the dominating technology for complex oxide compounds for magnetic-bubble devices and for magnetooptic applications. However, it was overlooked for the field of high-T_c superconductivity. Further technological developments and international collaboration in the complex area of liquid phase epitaxy are urgently needed to accelerate the progress of thin film applications of high-temperature superconductivity.

Acknowledgements

Discussions with T. Nishinaga, encouragement from S. Miyazawa and F.-K. Reinhart, and support from NTT and the Swiss National Science Foundation are gratefully acknowledged.

References

[1] H.J. Scheel, Appl. Phys. Lett. 37 (1980) 70.
[2] H.J. Scheel, G. Binnig and H. Rohrer, J. Cryst. Growth 60 (1982) 199.
[3] A. Chernov and H.J. Scheel, J. Cryst. Growth 149 (1995) 187.
[4] C. Klemenz and H.J. Scheel, J. Cryst. Growth 129 (1993) 421.
[5] M. Hawley, I.D. Raistrick, J.G. Beery and R.J. Houlton, Science 251 (1991) 1587.
[6] C. Gerber, D. Anselmetti, J.G. Bednorzz, J. Mannhart and D.G. Schlom, Nature 350 (1991) 279.
[7] H.P. Lang, H. Haefke, G. Leemann and H.J. Güntherodt, Physica C 194 (1992) 81.
[8] H.J. Scheel, C. Klemenz, F.K. Reinhart, H.P. Lang and H.J. Güntherodt, Appl. Phys. Lett. 65 (1994) 901.
[9] P. Bennema and J.P. van der Eerden, in: Morphology of Crystals, Ed. I. Sunagawa (Terra Scientific, Tokyo, 1987) ch. 1.
[10] G.H. Gilmer and K.A. Jackson, in: Crystal Growth and Materials, Ed. E. Kaldis and H.J. Scheel (North-Holland, Amsterdam, 1977) ch. 1.2.
[11] D. Sh. Tsagareishvili, G.G. Gvelesiani, I.B. Baratashvili, G.K. Moiseev and N.A. Vatolin, Russ. J. Phys. Chem. 64 (1990) 1404.
[12] G.K. Moiseev, N.A. Vatolin, S.I. Zaizeva, N.I. Ilyinych, D.S. Tsagareishvili, G.G. Gvelesiani, I.B. Baratashvili and J. Sestàk, Thermochim. Acta 198 (1992) 267.
[13] H.J. Scheel, MRS Bull. 19 (1994) 26.
[14] F.C. Frank, Acta Cryst. 4 (1951) 497.
[15] Y. Gotoh and H. Komatsu, J. Cryst. Growth 54 (1981) 163.
[16] W.K. Burton, N. Cabrera and F.C. Frank, Trans. R. Soc. A 243 (1951) 299.
[17] N. Cabrera and M.M. Levine, Phil. Mag. 1 (1956) 450.
[18] B. Mutaftschiev, in: Dislocations in Solids, Ed. F.R.N. Nabarro (North-Holland, Amsterdam, 1980) ch. 19, p. 90.
[19] B. van der Hoek, J.P. van der Eerden and P. Bennema, J. Cryst. Growth 56 (1982) 621.
[20] D. Elwell and H.J. Scheel, Crystal Growth from High-Temperature Solutions (Academic Press, London, 1975) ch. 3, p. 146; ch. 4, p. 157; ch. 6.
[21] P. Görnert, K. Fischer and C. Dubs, J. Cryst. Growth 128 (1993) 751.
[22] P. Hartman and W.G. Perdok, Acta Cryst. 8 (1955) 49; 521; 525.

[23] K.A. Jackson, in: Growth and Perfection of Crystals (Wiley, New York, 1958).
[24] B.N. Sun, P. Hartman, C.F. Woensdregt and H. Schmid, J. Cryst. Growth 100 (1990) 605.
[25] L.E.C. van de Leemput, P.J.M. van Bentum, F.A.J.M. Driessen, J.W. Gerritsen, H. van Kempen, L.W.M. Schreurs and P. Bennema, J. Cryst. Growth 98 (1989) 551.
[26] Y. Yamada, M. Nakamura, Y. Shiohara and S. Tanaka, J. Cryst. Growth 148 (1995) 241.
[27] M. Mukaida and S. Miyazawa, Jpn. J. Appl. Phys. 31 (1992) 3317.
[28] S.J. Pennycook, M.F. Chisholm, D.E. Jesson, R. Feenstra, S. Zhu, X.Y. Zheng and D.J. Lowndes, Physica C 202 (1992) 1.
[29] J. Summhammer, K. Kundzins, G. Samadi Hosseinali, R.M. Schalk, H.W. Weber, S. Proyer, E. Stangl and D. Bäuerle, Physica C 242 (1995) 127.
[30] H.J. Scheel, in: Advances in Superconductivity VI, Proc. ISS'93 Hiroshima (Springer, Tokyo, 1994) p. 29.
[31] M. Mukaida, S. Miyazawa and M. Sasaura, Jpn. J. Appl. Phys. 30 (1991) L1474.
[32] D.H. Lowndes, X.-Y. Zheng, S. Zhu, J.D. Budai and R.J. Warmack, Appl. Phys. Lett. 61 (1992) 852.
[33] H.J. Scheel and D. Elwell, J. Cryst. Growth 12 (1972) 153.
[34] A.A. Chernov, Sov. Phys. Usp. 4 (1961) 129.
[35] A.A. Chernov, Sov. Phys. Cryst. 8 (1963) 63.
[36] T. Nishinaga and H.J. Scheel, Proc. ISS'95 (Springer, Tokyo, 1996), accepted.
[37] H.J. Scheel, M. Berkowski and B. Chabot, J. Cryst. Growth 115 (1991) 19.
[38] A. Erbil and H.J. Scheel, unpublished.
[39] M.H. Grabow and G.H. Gilmer, Surf. Sci. 194 (1988) 333.
[40] M. Yoshida, T. Nakamoto, T. Kitamura, O.-B. Hyun, I. Hirabayashi, S. Tanaka, A. Tsuzuki, Y. Sugawara and Y. Ikuhara, Appl. Phys. Lett. 65 (1994) 1714.
[41] H.J. Scheel, W. Sadowski and L. Schellenberg, Supercond. Sci. Technol. 2 (1989) 17.
[42] M. Berkowski, P. Bowen, T. Liechti and H.J. Scheel, J. Am. Ceram. Soc. 75 (1992) 1005.
[43] P. Berberich, B. Utz, W. Prusseit and H. Kinder, Physica C 219 (1994) 497.